PNAS BRIEF REPORT | PHYSICS OPEN ACCESS

Superconducting critical temperature elevated by intense magnetic fields

Z. Wu[a], H. Chen[a], T. I. Weinberger[a], A. Cabala[b], D. E. Graf[c], Y. Skourski[d], W. Xie[e], Y. Ling[e], Z. Zhu[e], V. Sechovský[b], M. Vališka[b], F. M. Grosche[a], and A. G. Eaton[a,1]

Edited by Anthony Leggett, University of Illinois at Urbana-Champaign, Urbana, IL; received October 25, 2024; accepted December 4, 2024

Below a critical temperature T_c, superconductors transport electrical charge without dissipative energy losses. The application of a magnetic field B generally acts to suppress T_c, up to some critical field strength at which $T_c \rightarrow 0$ K. Here, we investigate magnetic field–induced superconductivity in high-quality specimens of the triplet superconductor candidate UTe_2 in pulsed magnetic fields up to $B = 70$ T. Strikingly, we find that this material has a higher T_c when $B > 40$ T ($T_c \approx 2.4$ K) than it does for $B = 0$ T ($T_c = 2.1$ K). This observation points to a fundamentally distinct mechanism for the formation of superconductivity at high B in UTe_2 compared to the case of $B = 0$ T.

triplet superconductor | high magnetic field | heavy fermion

The heavy fermion paramagnet UTe_2 exhibits numerous signatures of odd-parity (spin-triplet) superconductive pairing. These include high upper critical field strengths in excess of the Pauli pair-breaking limit for all orientations of B, along with only small changes in the NMR Knight shift upon crossing T_c (1, 2). Initial investigations of the superconductive properties of UTe_2 studied samples grown by the chemical vapor transport technique with typical values of $T_c \approx 1.6$ K (3); subsequent optimization of a salt-flux growth technique has yielded higher quality specimens with $T_c = 2.1$ K (4, 5). Remarkably, under the application of large magnetic fields, UTe_2 exhibits two field-induced superconductive states (6). Thermodynamic evidence suggests that these phases are distinct from the ground state superconductivity found at $B = 0$ T (7, 8). The three superconductive phases of UTe_2 are typically referred to as SC1, SC2, and SC3. The highest field superconducting state (SC3) has been found to persist up to $B \approx 70$ T (9) and is acutely sensitive to the orientation of B. SC3 has been found to demonstrate a remarkable resilience against the introduction of crystalline disorder (10). Recent measurements have pointed toward the presence of quantum critical fluctuations at very high B as a likely explanation for this exotic superconductivity (11), reminiscent of the case of the ferromagnetic superconductor URhGe (12).

Results and Discussion

Here, we investigate the sensitivity to temperature and magnetic field tilt angle of the high-B SC3 superconducting phase in pristine quality UTe_2. We performed contacted and contactless electrical conductivity measurements (*Materials and Methods*) in steady and pulsed magnetic fields, up to a maximal value of $B = 70$ T. Measurements were performed at magnetic field tilt angles θ_{b-c}, defined as the angle of rotation from the crystallographic b axis toward the c axis.

We find that the maximal value of T_c^{SC3} is reached for $\theta_{b-c} \approx 35°$. In Fig. 1*A* we plot contactless conductivity measurements at this orientation of B for incremental temperatures. The transition to the SC3 phase is identified by a sharp dip in the derivative of the signal. This dip is still clearly visible at $T = 2.3$ K but is gone at $T = 2.5$ K. By plotting the extent of SC3 in B and T in Fig.1*C*, the dashed line extrapolates to indicate $T_c^{SC3} \approx 2.4$ K for this orientation of B. This is remarkable, given that for $B = 0$ T, $T_c^{SC1} = 2.1$ K (Fig. 1*D*).

We mapped the extent of SC3 at multiple orientations of B from $\theta_{b-c} = 21°$ up to $\theta_{b-c} = 46°$ (Fig. 2). We find that T_c^{SC3} exhibits a dome-like angular dependence, being only ≈0.6 K at $\theta_{b-c} = 21°$, extending up to ≈2.4 K at $\theta_{b-c} = 35°$, and then reducing down to ≈1.8 K at $\theta_{b-c} = 39°$. For $\theta_{b-c} \geq 45°$ we find that the SC3 transition is no longer observable at 0.7 K, setting the upper boundary of the 0.7 K isotherm in Fig. 2*E*.

Author affiliations: [a]Cavendish Laboratory, Department of Physics, University of Cambridge, Cambridge CB3 0HE, United Kingdom; [b]Faculty of Mathematics and Physics, Department of Condensed Matter Physics, Charles University, Prague 2 121 16, Czech Republic; [c]National High Magnetic Field Laboratory, Tallahassee, FL 32310; [d]Hochfeld-Magnetlabor Dresden (HLD-EMFL), Helmholtz-Zentrum Dresden-Rossendorf, Dresden 01328, Germany; and [e]Wuhan National High Magnetic Field Center, Wuhan 430074, China

Author contributions: V.S., M.V., F.M.G., and A.G.E. designed research; Z.W., H.C., T.I.W., A.C., D.E.G., Y.S., W.X., Y.L., Z.Z., M.V., and A.G.E. performed research; Z.W. analyzed data; and A.G.E. wrote the paper.

The authors declare no competing interest.

[1]To whom correspondence may be addressed. Email: alex.eaton@phy.cam.ac.uk.

Published January 8, 2025.

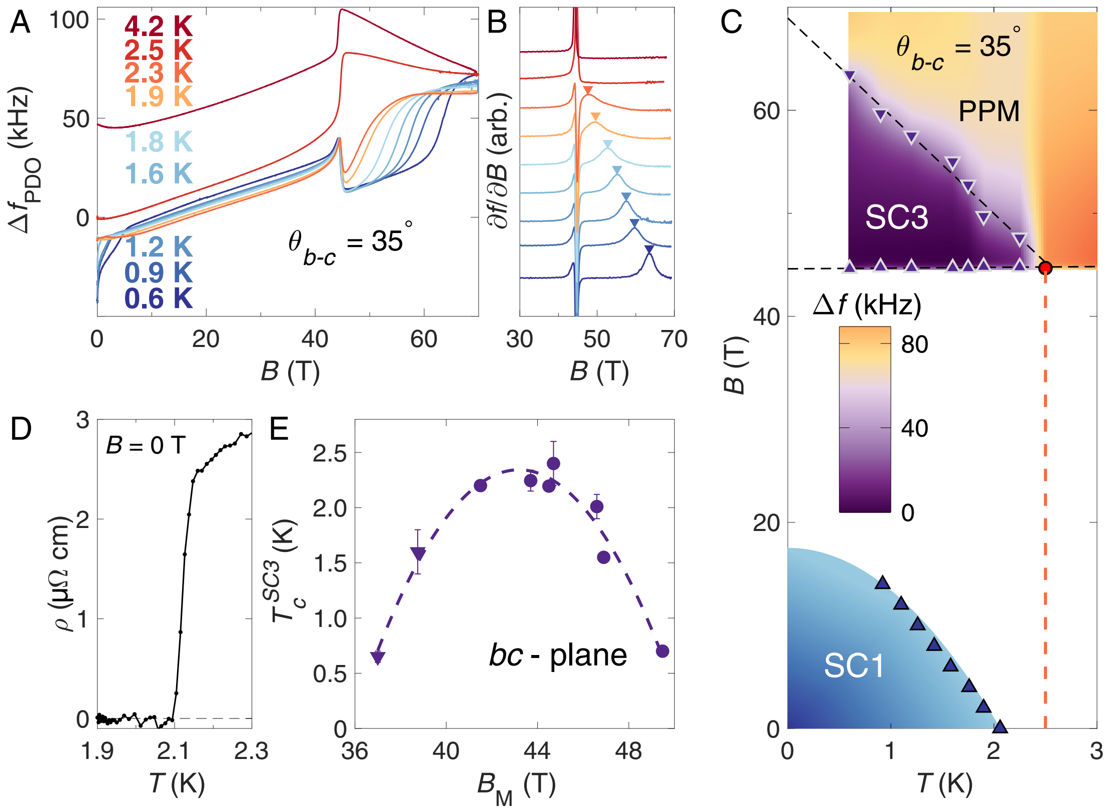

Fig. 1. Enhancement of T_c^{SC3} above T_c^{SC1}. (*A*) Pulsed field contactless conductivity measurements by the PDO technique (*Materials and Methods*) at incremental temperatures as indicated. The pronounced jump in the PDO signal at $B \approx 45$ T is due to a sudden increase in resistivity upon entering the polarized paramagnetic (PPM) state at the two highest measured temperatures, and due to the sudden onset of zero resistivity at all other (lower) temperatures as the SC3 state is accessed. (*B*) Derivatives with respect to B of the data from panel (*A*). (*C*) The phase diagram of SC1 and SC3 for $\theta_{b-c} = 35°$, using the data from panel (*A*) to define the SC3 region. Note that the SC2 phase is not present at this tilt orientation of B(5). Dashed lines are given as a guide to the eye. Points for the termination of SC3 are taken from the arrows in panel (*B*) and plotted as "down" triangles, while "up" triangles are from the sharp onset of SC3 located at $B \approx 45$ T for each of these temperatures. The extrapolation indicates that $T_c^{SC3} \approx 2.4$ K for this orientation of B. (*D*) Contacted resistivity measurement at $B = 0$ T showing that $T_c^{SC1} = 2.1$ K. (*E*) The dome-like angular profile of T_c^{SC3} plotted as a function of metamagnetic transition field B_{M} for rotations in the $b - c$ plane, in which B_{M} evolves as $1/\cos\theta_{b-c}$ (9). Triangular points are from contacted transport in steady fields, with circular symbols from contactless conductivity measurements in pulsed fields.

We note that all temperatures quoted for pulsed field measurements were determined immediately before the pulse. These temperature values are therefore lower bounds on the actual temperature of the sample during the measurement, which may undergo some heating from eddy currents and vortex motion caused by the rapid rate of change of B.

The observation of superconducting critical temperature being elevated by the application of a magnetic field is highly unusual. In the case of the related material URhGe, the observation of $T_c(B = 0 \text{ T}) < T_c(B > 0 \text{ T})$ was associated with the proximity to a B-induced quantum critical end point (12) located at $B \sim 10$ T. What is remarkable about the case of UTe_2 is that the high-B superconductivity extends up to $B \approx 70$ T (9). Preliminary experiments indicate that a similar mechanism of quantum criticality driving B-induced superconductivity appears to also be at play in UTe_2 (11).

Materials and Methods

UTe_2 single crystals were grown in a salt flux (4) using the methodology detailed in ref. 13. Samples were screened for quality by a combination of residual resistivity, magnetic susceptibility, and specific heat capacity measurements. High-quality specimens were then oriented by X-ray Laue diffractometry.

Contacted electrical conductivity measurements were performed by the four-probe technique, with ac current sourced along the a direction at low frequencies (<50 Hz). Contactless conductivity was measured by the proximity detector oscillator (PDO) method, by the same methodology as our previous measurements reported in ref. 14. This involves tracking the change in frequency of the PDO circuitry, Δf_{PDO}, which relates to changes in the skin depth, resistivity, and susceptibility of the sample (15). All PDO data presented in this study were acquired on down-sweeps of magnetic field pulses, which possess a much more gradual rate of change of magnetic field strength with respect to time than the up-sweeps. Data from Hochfeldlabor-Dresden (HLD) were acquired on the same sample utilizing an identical experimental setup (but different angular orientation with respect to B) as that reported in our prior quantum interference study (14), where the excellent Lifshitz–Kosevich fitting of oscillatory amplitudes with respect to temperature gives strong confidence that the sample temperature remained close to equilibrium during the down-sweep of the magnetic field pulse.

Data, Materials, and Software Availability. The datasets supporting the findings of this study are available from the University of Cambridge Apollo Repository (16).

ACKNOWLEDGMENTS. This project was supported by the Engineering and Physical Sciences Research Council (EPSRC) of the United Kingdom (grant no. EP/X011992/1). A portion of this work was performed at the National High Magnetic Field Laboratory, which is supported by NSF Cooperative Agreement No. DMR-2128556 and the State of Florida. We acknowledge support of the Hochfeld-Magnetlabor Dresden (HLD) at Helmholtz Zentrum Dresden

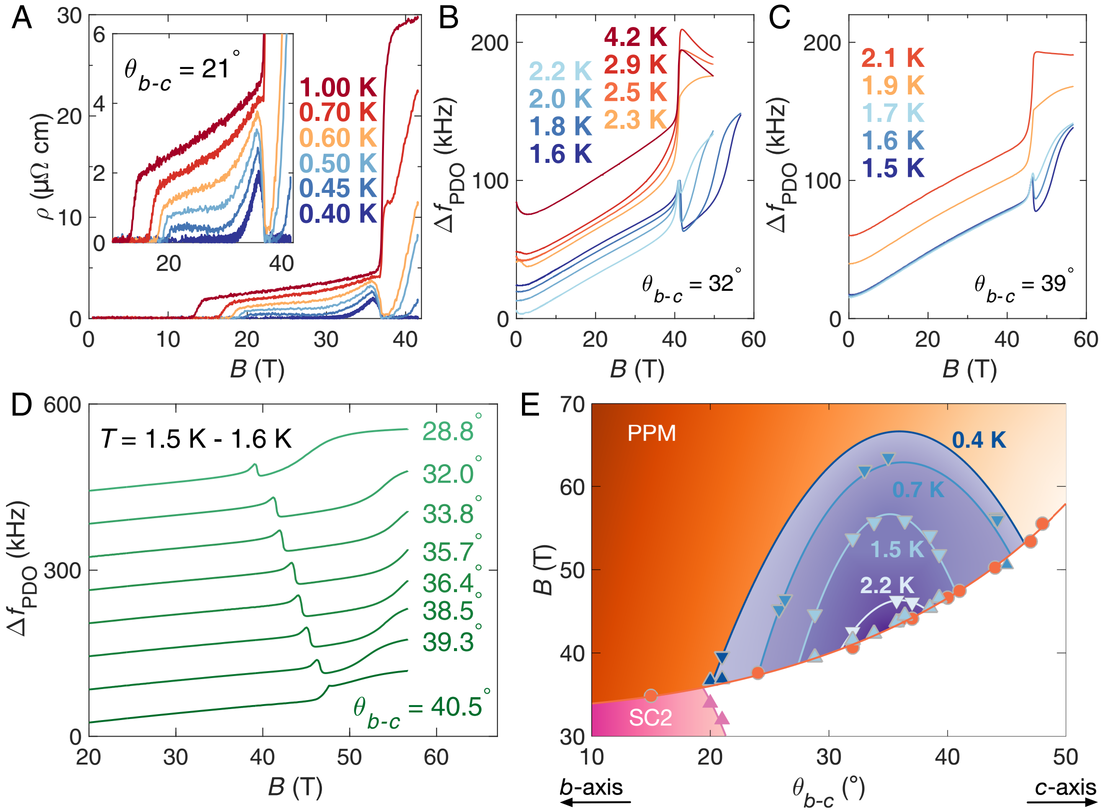

Fig. 2. Angular evolution of T_c^{SC3}. (*A*) Contacted resistivity data measured in static fields showing that at $\theta_{b-c} = 21°$, $T_c^{SC3} \approx 0.6$ K. The sharp upturn in ρ is characteristic of accessing the PPM state (in the absence of coexisting superconductivity). (*B*) Pulsed field contactless conductivity data showing that at $\theta_{b-c} = 32°$ $T_c^{SC3} \approx 2.2$ K while (*C*) at $\theta_{b-c} = 39°$, $T_c^{SC3} \approx 1.8$ K. (*D*) Isothermal rotation data showing the termination of SC3 for $\theta_{b-c} \gtrapprox 40°$ at $T \approx 1.5$ K. (*E*) Angular phase diagram of UTe_2 at high B, showing the temperature evolution of SC3 in the $b-c$ rotational plane. The polarized paramagnetic (PPM) and SC2 phases are also indicated, with points from ref. 5. Isotherm curves indicating the temperature domain of SC3 are drawn as guides to the eye, with quoted temperatures accurate to within approximately 0.1 K. The 0.4 K isotherm is constrained by measurements in steady fields at low θ_{b-c}, and extrapolated from the angular evolution of T_c^{SC3} observed at higher T in our pulsed field experiments at high θ_{b-c}, which we include for illustrative purposes. The evolution of T_c^{SC3} with θ_{b-c} appears to be reasonably symmetric either side of $\theta_{b-c} = 35°$.

Rossendorf (HZDR), a member of the European Magnetic Field Laboratory (EMFL). Crystal growth and characterization were performed in the Materials Growth and Measurement Laboratory, Charles University, Prague (https://mgml.eu/), which is supported within the program of Czech Research Infrastructures (project no. LM2023065). We acknowledge financial support by the Czech Science Foundation, project No. 22-22322S. T.I.W. acknowledges support from EPSRC studentship EP/R513180/1. T.I.W. and A.G.E. acknowledge support from QuantEmX grants from Institute for Complex Adaptive Matter (ICAM) and the Gordon and Betty Moore Foundation through Grants GBMF5305 and GBMF9616 and from the US NSF Grant Number 2201516 under the Accelnet program of Office of International Science and Engineering. D.V.C. acknowledges financial support from the National High Magnetic Field Laboratory through a Dirac Fellowship, which is funded by the NSF (Grant No. DMR-1644779) and the State of Florida. A.G.E. acknowledges support from the Henry Royce Institute for Advanced Materials through the Equipment Access Scheme enabling access to the Advanced Materials Characterisation Suite at Cambridge, grant numbers EP/P024947/1, EP/M000524/1, and EP/R00661X/1; and from Sidney Sussex College (University of Cambridge).

1. D. Aoki *et al.*, Unconventional superconductivity in UTe_2. *J. Phys. Condens. Matter* **34**, 243002 (2022).
2. S. K. Lewin, C. E. Frank, S. Ran, J. Paglione, N. P. Butch, A review of UTe_2 at high magnetic fields. *Rep. Prog. Phys.* **86**, 114501 (2023).
3. S. Ran *et al.*, Nearly ferromagnetic spin-triplet superconductivity. *Science* **365**, 684–687 (2019).
4. H. Sakai *et al.*, Single crystal growth of superconducting UTe_2 by molten salt flux method. *Phys. Rev. Mater.* **6**, 073401 (2022).
5. Z. Wu *et al.*, Enhanced triplet superconductivity in next-generation ultraclean UTe_2. *Proc. Natl. Acad. Sci. U.S.A.* **121**, e2403067121 (2024).
6. S. Ran *et al.*, Extreme magnetic field-boosted superconductivity. *Nat. Phys.* **15**, 1250–1254 (2019).
7. A. Rosuel *et al.*, Field-induced tuning of the pairing state in a superconductor. *Phys. Rev. X* **13**, 011022 (2023).
8. R. Schönemann *et al.*, Sudden adiabaticity signals reentrant bulk superconductivity in UTe_2. *PNAS Nexus* **3**, pgad428 (2024).
9. T. Helm *et al.*, Field-induced compensation of magnetic exchange as the possible origin of reentrant superconductivity in UTe_2. *Nat. Commun.* **15**, 37 (2024).
10. C. E. Frank *et al.*, Orphan high field superconductivity in non-superconducting uranium ditelluride. *Nat. Commun.* **15**, 3378 (2024).
11. Z. Wu *et al.*, A three-dimensional quantum critical phase boundary. arXiv [Preprint] (2024). https://arxiv.org/html/2403.02535v2 (Accessed 1 December 2024).
12. F. Lévy, I. Sheikin, A. Huxley, Acute enhancement of the upper critical field for superconductivity approaching a quantum critical point in URhGe. *Nat. Phys.* **3**, 460–463 (2007).
13. A. G. Eaton *et al.*, Quasi-2D Fermi surface in the anomalous superconductor UTe_2. *Nat. Commun.* **15**, 223 (2024).
14. T. I. Weinberger *et al.*, Quantum interference between Quasi-2D fermi surface sheets in UTe_2. *Phys. Rev. Lett.* **132**, 266503 (2024).
15. M. M. Altarawneh, C. H. Mielke, J. S. Brooks, Proximity detector circuits: An alternative to tunnel diode oscillators for contactless measurements in pulsed magnetic field environments. *Rev. Sci. Inst.* **80**, 066104 (2009).
16. Z. Wu *et al.*, Research data supporting: Superconducting critical temperature elevated by intense magnetic fields (2024). University of Cambridge Repository. https://doi.org/10.17863/CAM.113958. Deposited 10 December 2024.